frontiers | Frontiers in Earth Science

TYPE Original Research
PUBLISHED 29 November 2024
DOI 10.3389/feart.2024.1501183

OPEN ACCESS

EDITED BY
Jiangyu Wu,
China University of Mining and Technology, China

REVIEWED BY
Xiao Wang,
Shandong University of Science and Technology, China
Tao Zhang,
Nantong University, China
Xiaoxiao Cao,
Kyushu University, Japan

*CORRESPONDENCE
Chuanxin Rong,
chxrong@aust.edu.cn

RECEIVED 24 September 2024
ACCEPTED 04 November 2024
PUBLISHED 29 November 2024

CITATION
Feng J, Rong C, Shi H, Wang B, Wang Z, Guo L, Tu Z, Long W, Wu D and Wang X (2024) Study on strength and constitutive model of frozen calcareous clay under multi-factor interaction.
Front. Earth Sci. 12:1501183.
doi: 10.3389/feart.2024.1501183

Study on strength and constitutive model of frozen calcareous clay under multi-factor interaction

Jihao Feng[1], Chuanxin Rong[1]*, Hao Shi[1], Bin Wang[1], Zhi Wang[2], Longhui Guo[1], Zhuo Tu[1], Wei Long[1], Dong Wu[1] and Xueyan Wang[1]

[1]School of Civil Engineering and Architecture, Anhui University of Science and Technology, Huainan, China, [2]Anhui Water Conservancy Technical College, School of Civil Engineering and Architecture, Hefei, Anhui, China

The investigation into the complex mechanical properties of frozen calcareous clay under multi-factor interaction holds significant importance for the reliability and durability of engineering in cold regions. This study investigates the strength properties of frozen calcareous clay under different interaction levels by designing a four-factor, four-level orthogonal test that incorporates temperature, confining pressure, dry density, and water content. The study aimed to assess the sensitivity of each factor to failure stress, and establish an intrinsic model based on the Duncan-Chang model considering temperature, confining pressure, and water content. The results indicated that the stress-strain curves exhibit strain-hardening characteristics across various interaction levels. These curves can be divided into elastic and elastic-plastic phases, with the slope of the elastic phase and the stress value at the inflection point increasing with decreasing temperature and increasing confining pressure. When the confining pressure is maintained constant, the failure stress is negatively correlated with temperature. When the temperature is maintained constant, the failure stress is positively correlated with confining pressure. Sensitivity analysis shows that the influence of each factor on failure stress is as follows: temperature > confining pressure > dry density > water content. Additionally, the influence of temperature and confining pressure on failure stress is markedly greater than that of water content and dry density. The evolution of unfrozen water content follows three stages: sharp reduction, rapid reduction, and slow reduction. Verification against experimental data confirmed that the modified constitutive model effectively reflects the stress-strain relationship of frozen calcareous clay under the interaction of multiple factors.

KEYWORDS

frozen calcareous clay, interaction, strength characteristics, unfrozen water content, modified duncan-chang constitutive model

1 Introduction

The strength and deformation of permafrost are critical mechanical characteristics of soil that significantly affect engineering designs in cold regions (Shi et al., 2024; Long et al., 2024; Hai et al., 2024). Permafrost is a four-phase system comprising solid mineral particles, ice crystals, liquid water, and gas. Its strength is influenced by factors such as temperature, soil type, and stress state (Hu and Wang, 2013; Xu et al., 2020). It is worth noting that the deformation of permafrost directly impacts the stability and safety of engineering structures subjected to freeze-thaw cycles (Xu et al., 2017; Kong et al., 2017). Therefore, in the engineering design of cold regions, it is crucial to accurately evaluate the strength and deformation of frozen soil to ensure the reliability and durability of the project (Bai et al., 2018; Tatsuoka et al., 2008; Lu et al., 2019). This evaluation holds significant engineering importance for the design and construction of projects in these regions (Duriez and Vincens, 2015; Ni et al., 2018; Hoyos et al., 2014).

The mechanical properties of permafrost are influenced by various factors (Horpibulsuk et al., 2007; Ma et al., 2021; Liu and Carter, 2003), prompting extensive research under different conditions. Temperature, a crucial factor in the formation and stability of permafrost, significantly impacts its mechanical properties (Cudmani et al., 2022). As temperature decreases, water within the soil body freezes into ice, reconstructing the soil's microstructure and markedly increasing its strength and stiffness. Confining pressure is another critical factor affecting the mechanical properties of permafrost (Sun et al., 2022). Increased confining pressure enhances particle contact and alters the pore structure within the soil, influencing its mechanical response. Under high confining pressures, permafrost exhibits more complex non-linear strength and deformation characteristics. Additionally, dry density, an indicator of soil compactness, directly affects the contact area and force between soil particles, thereby determining the mechanical properties of permafrost (Li et al., 2023). Water content also plays a significant role in the mechanical behavior of frozen soils (Wu et al., 2021). Adequate water content can form an effective ice cementation network during freezing, enhancing the strength and stability of permafrost. Conversely, excessive water content can increase pore water pressure and diminish the mechanical properties of permafrost. These factors not only act independently but also interact synergistically to determine the mechanical behavior of permafrost.

With the rapid advancements in measurement and analysis methods, substantial improvements have been made in understanding the mechanical properties of cryogenic soil under various environmental conditions. Researchers have focused on detailing the complex deformation and failure mechanisms of these soils. Despite these efforts, achieving a comprehensive and predictive model for the deformation, strength, and failure behaviors of cryogenic soil remains a critical challenge. Formulating a precise constitutive relation equation and failure criterion is essential for this task. Suebsuk et al. (2010) developed a generalized constitutive model that can be applied to disturbed clay, natural state clay, and artificially reshaped clay. This model integrates plastic behavior to clarify how structural factors influence the direction of plastic strain during both hardening and softening phases. Yang et al. (2010) carried out triaxial compression tests on frozen sand, examining the mechanical properties of soil under various confining pressures and water contents. They introduced a nonlinear Mohr-Coulomb criterion to analyze the strength of frozen sand and derived generalized values for the internal friction angle and cohesion based on experimental data. Liao et al. (2016) revealed the significant impact of soil composition, particularly salt content, on its mechanical properties. By applying a generalized nonlinear strength theory, Liao developed a strength criterion for frozen soil layers that accounts for variations in salt content. Through conventional triaxial testing, Liao proposed a modified hydrostatic pressure expression using the critical strength function from the modified Cam clay model's meridian plane.

In summary, previous studies have explored the mechanical properties of frozen clays under variations in single or limited independent variables, establishing constitutive relationship equations and damage criteria. However, there is a notable lack of research on frozen calcareous clay under multifactor interactions. Given the complexity of the mechanical properties of frozen soils in diverse and variable natural environments, the current practice of analyzing each factor in isolation using the control variable method is limited. This approach provides a relatively one-sided understanding of the mechanical properties of permafrost under multifactor interactions and fails to meet the stringent requirements for material durability in the extreme and variable conditions of cold region projects.

The purpose of this study is to elucidate the complex mechanical properties of frozen calcareous clay under multifactor interactions to provide a robust theoretical foundation and technical support for the safety and durability of engineering projects in cold regions. Consequently, a four-factor, four-level orthogonal test was designed to investigate calcareous clay under the interaction of temperature, confining pressure, water content, and dry density. This test aims to examine the evolution of failure stress and the influence of each factor under different interaction levels. Additionally, an ontological model of frozen calcareous clay based on the Duncan-Chang model, incorporating temperature, confining pressure, and water content, is proposed to predict its stress-strain relationship under multifactor interactions.

2 Experimental materials and test methods

2.1 Testing materials

The calcareous clay (CC) used in the test was sourced from a deep layer (420–430 m) of a coal mine in the Lianghuai mining area, northern Anhui Province, China. It was transported to the laboratory in sealed packaging. The basic physical and mechanical properties of the undisturbed soil samples are shown in Table 1. Following standard provisions (China Planning Press, 2019), the undisturbed soil was dried naturally. After drying, the soil was placed in an oven at 105° C for 12 h A crusher. The dried and processed lumpy soil is crushed once by a crusher. However, the particle size of the crushed soil did not meet the test requirements, necessitating secondary crushing. After the second crushing, the soil was sieved through a 0.5 mm sieve to obtain the desired particle size for the experiment. The crushing process is shown

10.3389/feart.2024.1501183

TABLE 1 Properties of deeply buried calcareous clay.

Types of soil samples	Soil sample depth/m	Water content/%	Wet density/(g/cm^3)	Dry density/(g/cm^3)	Void ratio	Liquid limit/%	Plastic limit/%	Unconfined compression strength/KPa
Calcareous clay	420–430	22.62	2.04	1.66	0.64	54	35	118.8

in Figure 1. The particle size distribution was measured using a laser particle size analyser (BT-2001) (He et al., 2024), with results presented in Figure 2. The analysis revealed that the particle size distribution of the calcareous clay primarily ranged from 0.5 to 450 microns, with a significant concentration between 25 and 180 microns. The cumulative content curve of the particle size distribution indicates a relatively stable slope, demonstrating a uniform texture and consistent particle size range within the calcareous clay. This uniformity is beneficial to ensure that the prepared sample has a consistent texture and is isotropic.

2.2 Test scheme

2.2.1 Orthogonal design

This study employed an orthogonal experimental design method to investigate the influence of temperature, pressure, moisture content, and dry density on calcareous clay. Each factor was set at four different levels, resulting in a total of 16 experimental groups, as outlined in Table 2. Each group of samples is configured with four influencing factors, which we denominate as 'multi-factor interaction'. In each group of samples, one factor is maintained constant, while the remaining factors are varied. The term 'interaction level' is employed to designate any set of experimental conditions. The dry density for each sample was calculated using the following expression (Wu et al., 2023):

$$\rho_d = \frac{m_1}{v} \tag{1}$$

$$m = m_1 + m_1 \times \omega \tag{2}$$

where m_1 is the mass of dry soil in a single specimen, g; ρ_d is the dry density of soil, g/cm^3; v is the sample volume, cm^3; m is the mass of sample, g; ω is water content, %.

2.2.2 Specimen preparation

The mass of dry soil and water required for each group of samples was calculated using Equations 1, 2. The dry soil and water were mixed evenly and placed in a sealed bag for 24 h to ensure uniform moisture content throughout the soil samples. Subsequently, the wet soil is filled into the 50 mm × 100 mm internal mold in five increments and compacted. During the first four compacting processes, complete compaction is not required. Instead, it is only necessary to ensure that sufficient space is left for the inclusion of subsequent layers of soil. Simultaneously, the surface of each layer of soil is scarified to enhance the bonding between the layers. The objective is to physically facilitate the interlocking of soil particles, thereby enhancing the overall structural stability (Zhang et al., 2021). Prior to the preparation of the samples, the molds were cleaned and an even layer of petroleum jelly was applied to their inner surfaces. This was done in order to facilitate the removal of the specimens from the molds during the demolding process. Post-compaction, the specimens and molds were sealed with cling film and placed in a cryostat at −20°C for 1 hour before demolding. Once demolded, the specimens were further sealed with cling film and frozen in the cryostat at −20°C for 24 h, followed by placement in a cryostat at the target temperature for an additional 24 h.

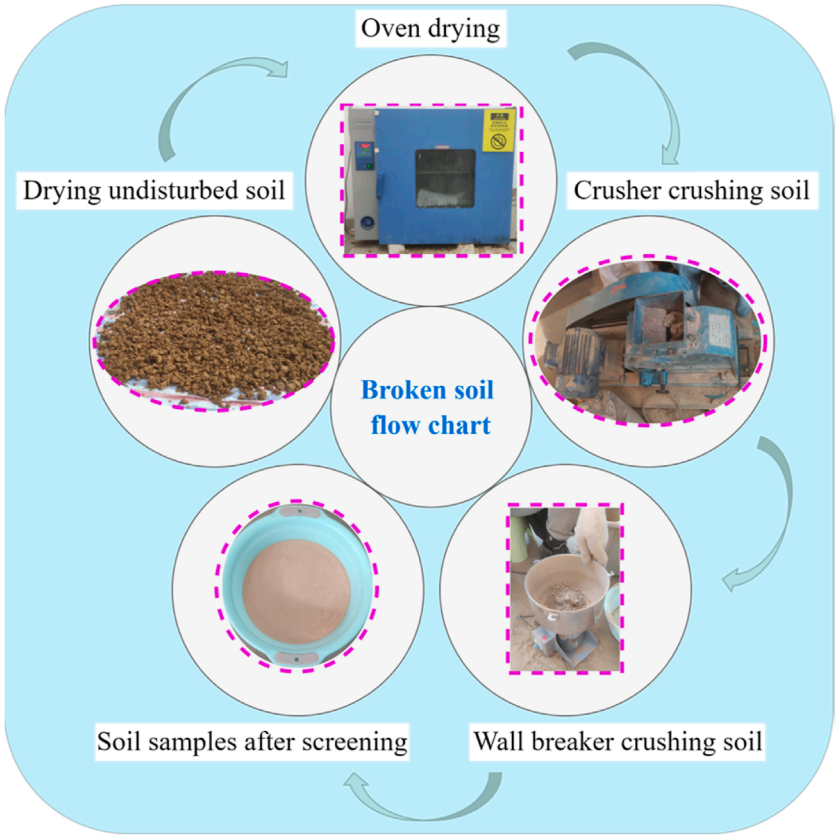

FIGURE 1
Test flow chart of drying and crushing of calcareous clay.

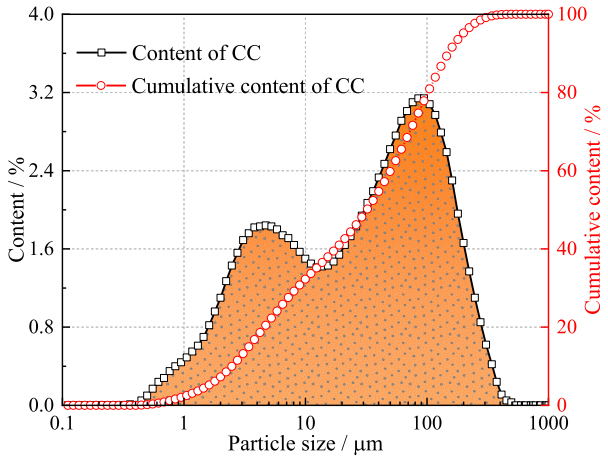

FIGURE 2
Particle size distribution of calcareous clay after crushing.

Figure 3 illustrates the microstructural characteristics of the calcareous clay post-sampling. Scanning electron microscope (SEM) analyses revealed no significant differences under varying conditions; hence, only the results for a sample with a dry density of 1.86 g/cm³ and a moisture content of 20% were analyzed. The texture of the unfrozen calcareous clay after preparation was uniform, with tightly bound soil particles and small pores, indicating high-quality sample preparation. In contrast, the frozen calcareous clay appeared relatively loose with tiny cracks, likely caused by the expansion force during the freezing of pore water into ice. Given that the SEM scans at 500 μm represent a magnification by a factor of 1,000, and the locations of the photographs were selectively chosen to highlight the most significant changes, the specimens were kept at negative temperatures during the test, and the ice filled these cracks. Therefore, the effects produced by the cracks after freezing can be considered negligible.

2.2.3 Testing procedures

Figure 4A illustrates the configuration of the low-temperature rock (soil) triaxial test system (ZTCR-2000, Changchun Development Test Instrument Co., Ltd., China), indicating that the test setup comprises a computer processing system, a low-temperature geotechnical triaxial test control system, a low-temperature geotechnical triaxial test machine, a hydraulic oil circulating pump, and an alcohol refrigerant circulating pump. A schematic diagram of the triaxial test system is presented in Figure 4B. It can be noted that the computer processing system is utilized to regulate the control system of triaxial test for low-temperature rock and soil. This system has the capability to

10.3389/feart.2024.1501183

TABLE 2 Orthogonal experimental design table.

Sample number	Temperature/°C	Confining pressure/MPa	Water content/%	Dry density/(g/cm^3)
A-1	−5	0.5	15	1.66
A-2	−5	1	17.5	1.86
A-3	−5	1.5	20	1.76
A-4	−5	2	12.5	1.56
B-1	−10	0.5	12.5	1.76
B-2	−10	1	20	1.56
B-3	−10	1.5	17.5	1.66
B-4	−10	2	15	1.86
C-1	−15	0.5	17.5	1.56
C-2	−15	1	15	1.76
C-3	−15	1.5	12.5	1.86
C-4	−15	2	20	1.66
D-1	−20	0.5	20	1.86
D-2	−20	1	12.5	1.66
D-3	−20	1.5	15	1.56
D-4	−20	2	17.5	1.76

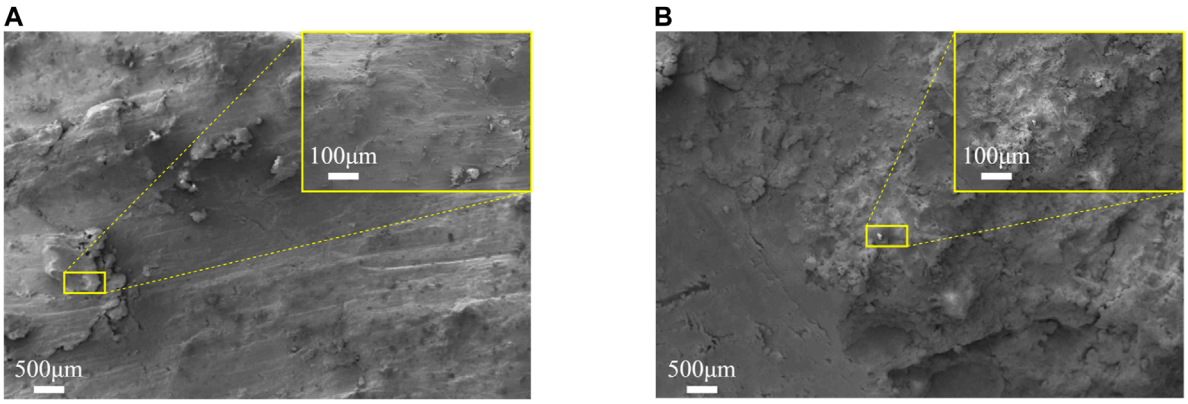

FIGURE 3
Scanning electron microscopy of calcareous clay samples after drying. **(A)** Unfrozen calcareous clay samples. **(B)** Frozen calcareous clay samples.

control the hydraulic oil circulating pump, which can provide the necessary axial and confining pressures for the low temperature rock and soil triaxial testing machine. Additionally, the alcohol refrigerant circulating pump is employed. The pump is furnished with an independent control switch, enabling the operator to decide whether to activate it flexibly in accordance with the actual requirements. The low temperature rock and soil triaxial testing machine is provided with axial and circumferential strain gauges and a geotechnical sensor located above the chamber for measuring the axial pressure. During the test, the axial pressure and the resulting axial and circumferential strain data of the specimen will be transmitted to the computer processing system in real time and displayed in the form of stress-strain curves. This greatly facilitates the testers' monitoring and analysis of the specimen's current status.

10.3389/feart.2024.1501183

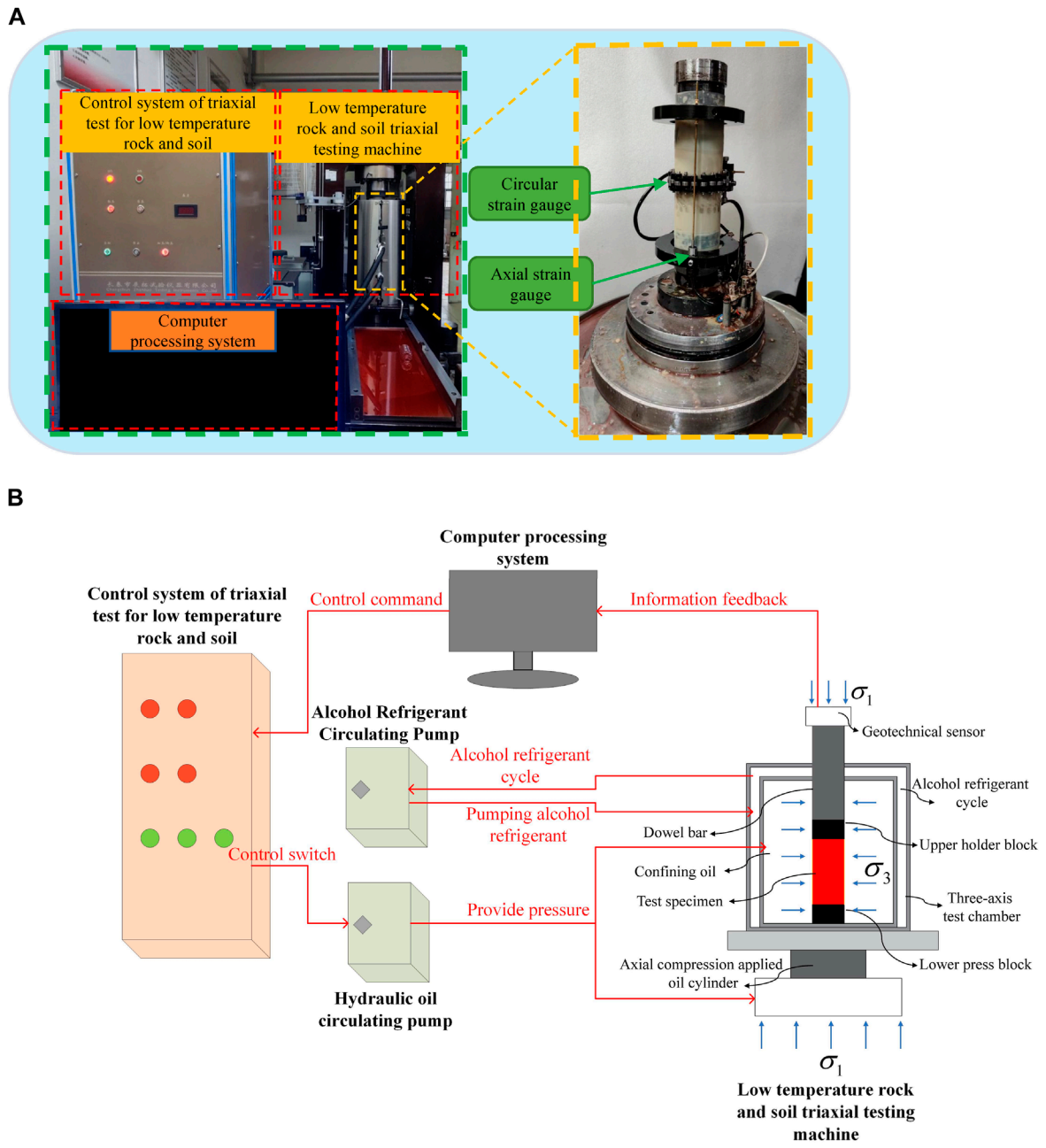

FIGURE 4
Low Temperature Geotechnical Triaxial Test System. **(A)** Configuration of low temperature geotechnical triaxial test system. **(B)** The schematic diagram of the working principle of low temperature geotechnical triaxial test system.

Before initiating the test, the temperature in the test chamber was adjusted to the target level, and the sample underwent a 2-h pre-cooling period. Following this, the sample was loaded into the chamber, and a prestress of 100 N was applied to secure it. The sample was then frozen for an additional 6 h to ensure it reached the target temperature at the commencement of the test. The stress path diagram for the triaxial test is presented in Figure 5, with preloading as the initial point. During both the preloading and freezing stages, only the 100 N prestress was applied to the specimen. Subsequent to the freezing stage, hydrostatic pressure was increased to achieve the target confining pressure, maintaining equal axial and confining pressures, thus ensuring a deviatoric stress of 0 MPa. After reaching the target pressure, it was stabilized for 30 min. Finally, axial loading was applied at a rate of 0.3 mm/min until the specimen failed (Coal Industry Press, 2011). Figure 6 illustrates the comparison of specimens before and after the test. It can be observed that the specimen experienced significant axial compression, resulting in a radial deformation characterized by an "hourglass" shape, with pronounced wrinkles appearing at both ends.

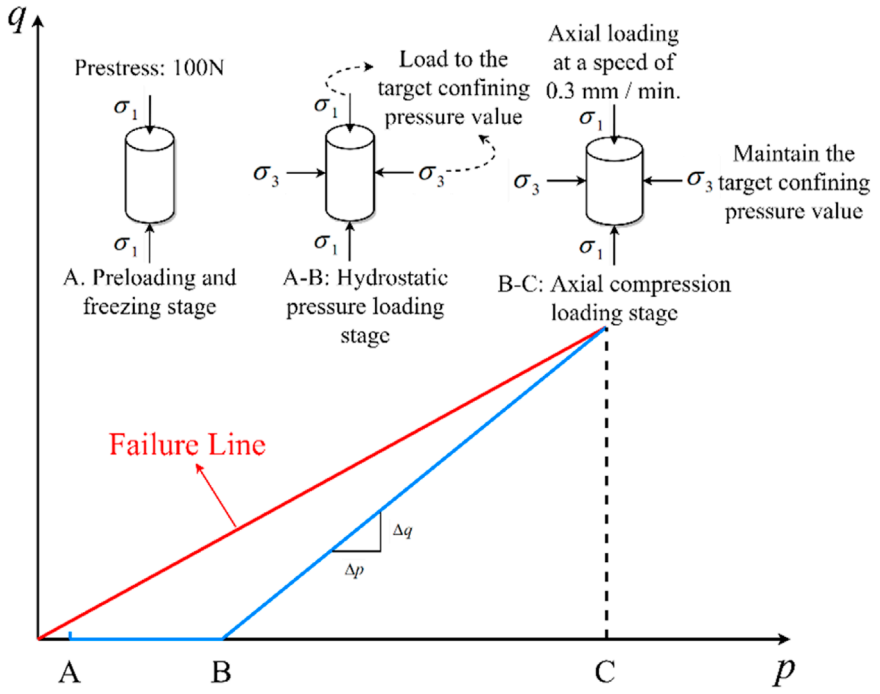

FIGURE 5
The stress path diagram and the stress change of the specimen during the triaxial test.

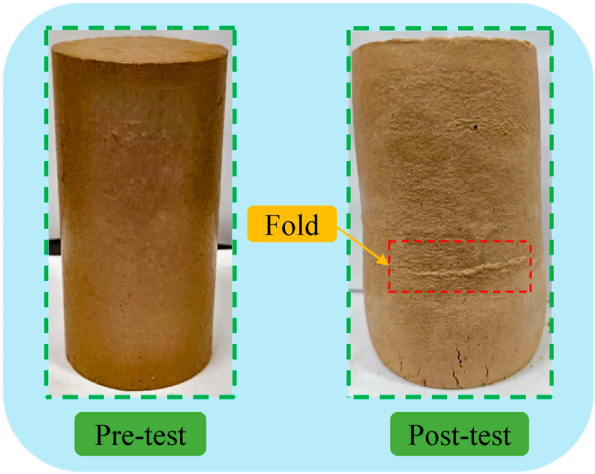

FIGURE 6
Comparison of changes of calcareous clay samples before and after test.

3 Test result analysis

3.1 Relationship between deviatoric stress and axial strain

The stress-strain curves of frozen calcareous clays at various temperatures are depicted in Figure 7 (In the figure $\sigma_1 - \sigma_3$ is the deviatoric stress and ε_1 is the axial strain). These curves exhibit strain-hardening characteristics across different interaction levels (Wu et al., 2017). Specifically, at −5°C and −10°C, the curves demonstrate weak hardening behavior, while at −15°C and −20°C, they exhibit general hardening behavior. The transition from weak to general hardening with decreasing temperature can be attributed to the gradual transformation of liquid water in the soil into solid ice crystal particles. This transformation enhances both the strength and strain-hardening characteristics of the soil body due to the increased cementing effect of the ice crystal particles (Shi et al., 2020).

Figure 8 schematically illustrates the microstructure and mechanical behavior of frozen calcareous clay (In the figure σ_3 is the confining pressure). Under axial and confining pressure, frozen calcareous clay experiences extrusion and friction between soil particles. During the freezing process, the transformation of liquid water into ice diminishes its lubricating effect. The formation of cementing ice tightly binds adjacent soil particles together, enhancing cohesion. Additionally, the presence of pore ice acts similarly to the addition of aggregates to cement, significantly increasing the strength of the calcareous clay (Wu et al., 2024; Wu et al., 2022).

The deviatoric stress-axial strain curves of frozen calcareous clay exhibit distinct elastic and elastoplastic phases, which can be elucidated through the following analysis: Initially, under the applied hydrostatic pressure for 30 min, the pore space within the sample undergoes compaction. Concurrently, the presence of cemented ice fosters a dense structure among soil particles. During this phase, the specimen's deformation modulus is substantial, leading to a rapid increase in preload with axial strain, characterized by a linear relationship. This behavior, which may originate from the presence

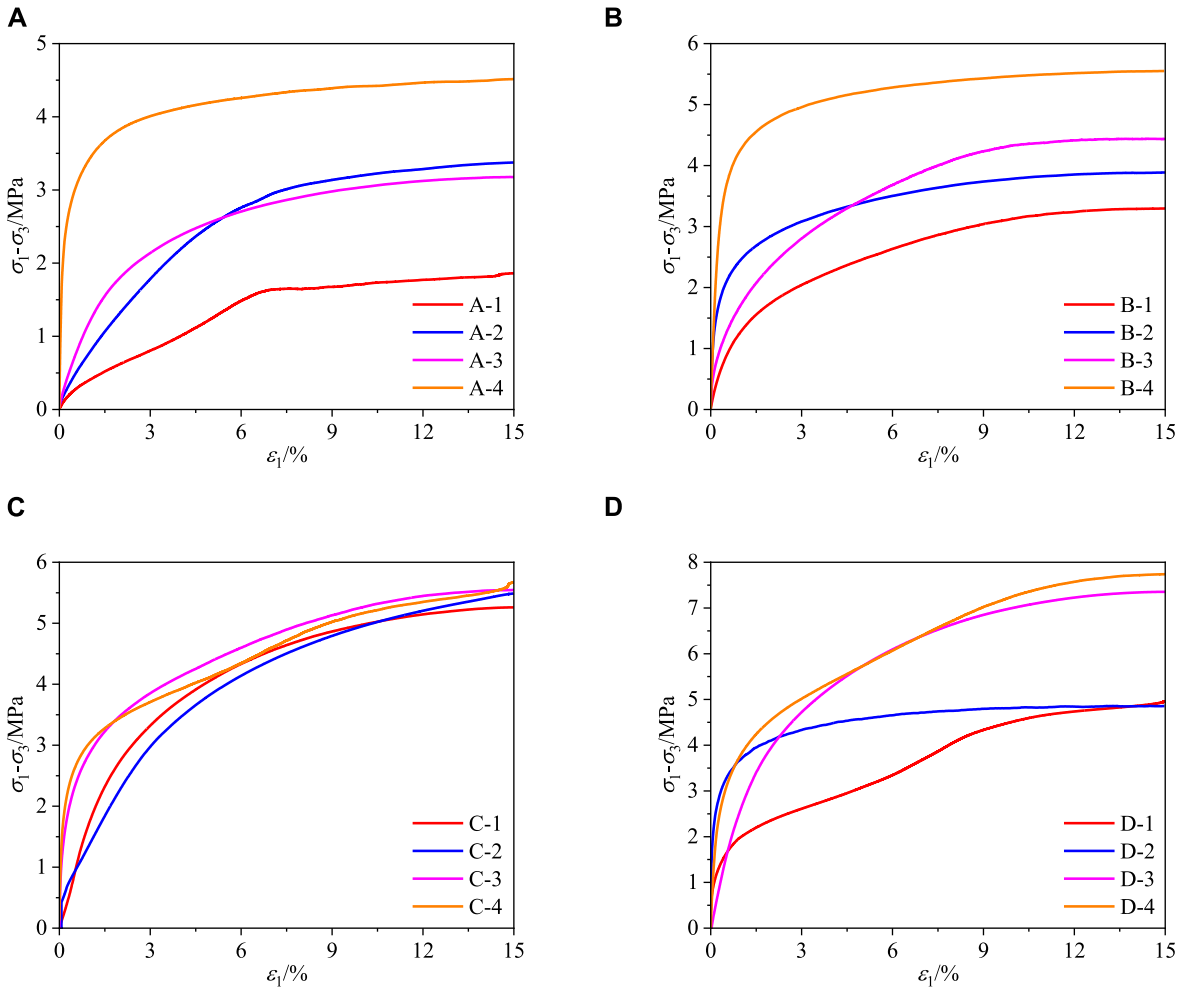

FIGURE 7
The deviatoric stress-axial strain curves of frozen calcareous clay at different temperatures. **(A)** T=−5°C. **(B)** T=−10°C. **(C)** T=−15°C. **(D)** T=−20°C.

of intact cemented ice and pore ice, reflects elastic properties. As axial strain continues to increase, the preload and axial strain exhibit non-linear growth. The slope of the curve, representing the deformation modulus, gradually diminishes and stabilizes, without exhibiting a distinct peak throughout the curve. At this stage, the internal cemented ice and pore ice within the specimen undergo compression or even disintegrate, leading to the gradual formation and expansion of internal cracks (Wu et al., 2020). Consequently, the specimen becomes damaged, the deformation modulus gradually decreases, and its resistance to deformation weakens (Zhang et al., 2024).

Figure 7 reveals that during the elastic phase, both the slope (modulus of elasticity) and stress value at the inflection point (Junction of elastic and elastoplastic phases) demonstrate an increasing trend with decreasing temperature and increasing confining pressure. This phenomenon may be attributed to several factors: Firstly, the decrease in temperature reduces the content of unfrozen water, thereby increasing the presence of cemented ice and pore ice. Consequently, the effects of cementation and "replacement" are amplified, leading to an augmentation in the specimen's deformation modulus. Secondly, the rise in confining pressure intensifies the external load on the specimen (Zhang et al., 2023). Microscopically, the pore space experiences further compaction due to the elevated confining pressure, resulting in closer contact between soil particles and increased compression and friction. Macroscopically, the specimens endure greater confining pressures, enhancing confinement and thereby augmenting their ability to resist deformation.

3.2 Sensitivity analysis of various factors on failure stress

Considering the strain-hardening nature of the stress-strain curves in this test, the deviator stress at an axial strain of 15% serves as the failure stress for analysis (China Planning Press, 2019). Figure 9A compares the results at different temperatures, indicating a gradual increase in the specimen's failure stress as temperature decreases, a trend that is pronounced. Under identical temperature conditions, the failure stress of the specimen exhibits a positive correlation with confining

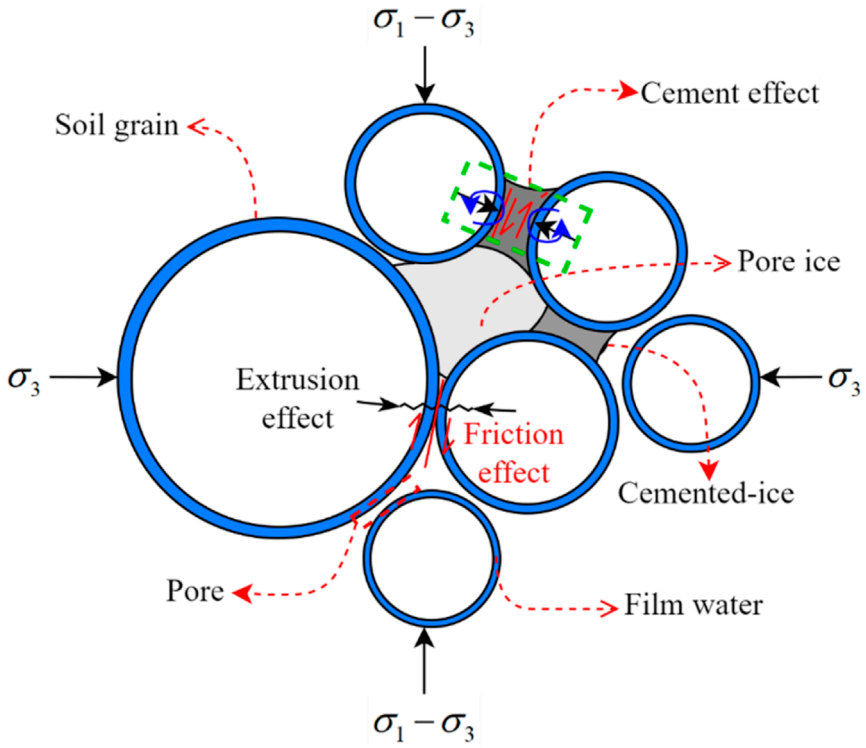

FIGURE 8
Microstructure and mechanical behavior of frozen calcareous clay particles.

pressure. Notably, at 5°C, the peak deviatoric stress of A-2 surpasses that of A-3. Analyzing A-2 and A-3 specimens reveals that A-2 has a dry density of 1.86g/cm3 and a moisture content of 17.5%, while A-3 has a dry density of 1.76g/cm3 and a moisture content of 20%. Although A-2 exhibits higher dry density compared to A-3, its moisture content is lower. The discrepancy in failure stress between A-2 and A-3 may originate from the fact that at 5°C, some free water within the specimen remains in liquid form despite freezing. It should be indicated that liquid water, while possessing a lubricating effect, weakens the cementation and "replacement" effect of ice, consequently diminishing the specimen's strength. However, the increase in dry density increases the number of soil particles in the specimen, reduces porosity, enhances effective contact area between particles, and intensifies extrusion and friction, thereby significantly improving compressive strength. Hence, at this temperature, the impact of water content on sample compressive strength is minimal compared to dry density.

In Figure 9B, at a moisture content of 17.5%, the failure stress of C-1 surpasses that of B-3, despite B-3 having higher confining pressure and dry density. This may be attributed to C-1 being at −15°C, where nearly all free water freezes and the process of bonded water freezing initiates. At this temperature, the lubricating effect of liquid water diminishes significantly, while the cementation and "replacement" effects of ice are greatly enhanced. This substantial enhancement in ice cementation and "replacement" significantly increases the compressive strength of the specimen. This observation aligns with the general hardening nature of the stress-strain curve at −15°C, underscoring the significant impact of temperature on failure stress magnitude.

Analysis of Figures 9B,C reveals a disordered distribution of failure stress under constant dry density and moisture content conditions. This suggests that while dry density and moisture content exert some influence on failure stress, their impact is almost negligible compared to temperature and confining pressure.

The test data acquired from orthogonal experiments (Jiang et al., 2021) are typically subjected to sensitivity analysis for data processing. This involves averaging the extreme differences in the target value influenced by each factor, thereby identifying the primary factors affecting the target value through the difference between the maximum and minimum test values (Deng et al., 2023). The sensitivity analysis results, presented in Table 3, indicate that temperature exhibits the most substantial effect on failure stress, with an extreme difference value of 2.99 MPa, while moisture content has the least impact, registering an extreme difference value of 0.78 MPa. The sensitivity ranking of each influencing factor on failure stress is as follows: temperature > pressure > dry density > moisture content. This hierarchy underscores that the influence of temperature and pressure on failure stress far surpasses that of moisture content and dry density. Thus, the pronounced effect of temperature and pressure on failure stress aligns with the earlier analysis.

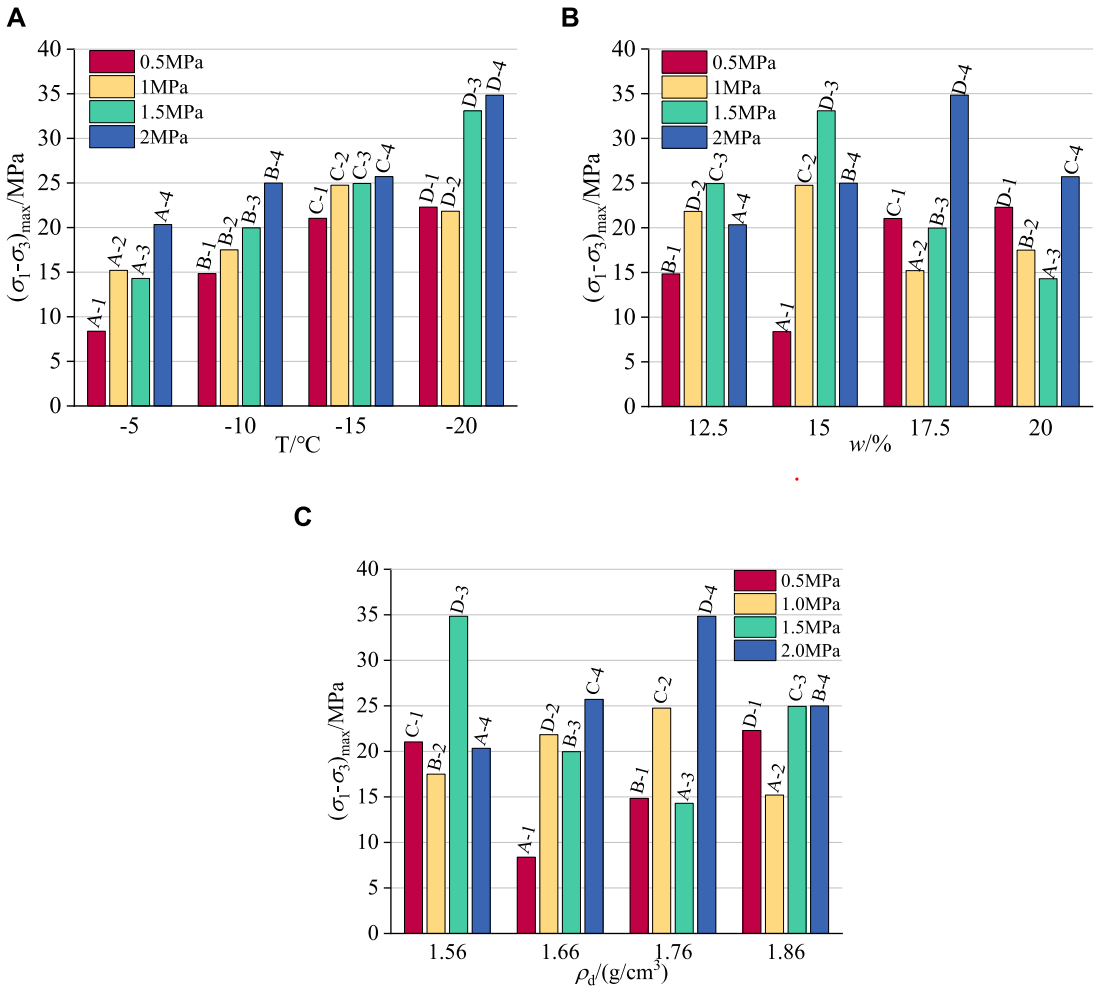

FIGURE 9
The failure stress histogram of frozen calcareous clay under various factors. **(A)** Temperature. **(B)** Moisture content. **(C)** Dry density.

4 Modified Duncan-Chang constitutive model of frozen calcareous clay

4.1 Determination of unfrozen water content calculation formula

Alterations in the unfrozen water content of permafrost, representing the phase transition between solid and liquid water directly affect the soil's mechanical properties (Pardo Lara et al., 2021; Wen et al., 2012). To investigate this phenomenon, an NMR test system was employed in this study to measure the unfrozen water content of the samples under the specified orthogonal test conditions. It was ensured that the temperature had reached the designated level and had stabilized for a minimum of 2 hours before conducting the measurements. The NMR test system setup is illustrated in Figure 10.

Figure 11 depicts the evolution of unfrozen water content concerning temperature, delineated into three distinct phases: (1) From 0°C to −2.7°C: Sharp Decrease Phase - As the temperature drops below the freezing point of the calcareous clay, the free water within the soil undergoes a rapid phase transition and rapid freezing. This abrupt change manifests as a sharp decline in unfrozen water content. (2) From −2.7°C to −11.5°C: Rapid Decrease Phase - Within this temperature range, any remaining free water in the soil continues its freezing process, leading to a significant reduction in unfrozen water content. (3) From −11.5°C to −25°C: Slow Reduction Stage - At this juncture, the free water in the soil is predominantly frozen, while the phase transition of bound water commences. Bound water, tightly adhering to soil particles due to capillary action, electrostatic adsorption, and surface tension, encounters difficulty in freezing (Wen et al., 2012). Consequently, the unfrozen water content diminishes gradually at a slower pace. In summary, the progressive decrease in temperature prompts the gradual freezing of free water within the soil, while the freezing of bound water occurs with greater resistance, resulting in the observed evolution of unfrozen water content across the described phases.

The quantity of unfrozen water content within permafrost significantly influences its strength, making the investigation of unfrozen water content essential (Chen et al., 2021; Zhang et al., 2020). To estimate the unfrozen water content, this study employs

TABLE 3 Sensitivity analysis of failure strength.

Sample number	Temperature/°C	Confining pressure/MPa	Water content/%	Dry density/(g/cm^3)	Breaking stress/MPa
A-1	−5	0.5	15	1.66	1.86
A-2	−5	1	17.5	1.86	3.38
A-3	−5	1.5	20	1.76	3.18
A-4	−5	2	12.5	1.56	4.52
B-1	−10	0.5	12.5	1.76	3.30
B-2	−10	1	20	1.56	3.89
B-3	−10	1.5	17.5	1.66	4.44
B-4	−10	2	15	1.86	5.55
C-1	−15	0.5	17.5	1.56	5.26
C-2	−15	1	15	1.76	5.50
C-3	−15	1.5	12.5	1.86	5.54
C-4	−15	2	20	1.66	5.68
D-1	−20	0.5	20	1.86	4.96
D-2	−20	1	12.5	1.66	4.86
D-3	−20	1.5	15	1.56	7.35
D-4	−20	2	17.5	1.76	7.74
R	2.99	2.03	0.78	1.05	

the empirical formula introduced by Xu et al. (2001). The amount of unfrozen water content can be calculated using the Equation 3:

$$\omega_u = \omega T_f{}^b T^{-b} \tag{3}$$

where ω_u is the unfrozen water content at -T°C, %; ω is the initial water content, %; T_f is the absolute value of the freezing temperature of the sample, °C; T is the absolute value of temperature, °C; b is the test constant.

According to the NMR test results, the starting freezing temperature of calcareous clay was identified as −0.8°C. The measured data were subjected to fitting, and the fit is illustrated in Figure 12. The fit appears to be satisfactory, with a correlation coefficient of R^2 = 0.97687. This high value suggests that the formula can effectively depict the relationship between the unfrozen water content of calcareous clay and the temperature and initial water content. Consequently, it can provide more accurate predictions of the unfrozen water content of calcareous clay.

$$\omega_u = 0.8^{0.54945}\omega T^{-0.54945} = 0.8846\omega T^{-0.54945} \tag{4}$$

4.2 Modified Duncan-Chang constitutive model

The Duncan-Chang model (Dong et al., 2023) employs hyperbolic equations to describe the stress-strain behavior of soil. The model can be mathematically expressed as follows:

$$\sigma_1 - \sigma_3 = \frac{\varepsilon_1}{\lambda + \nu\varepsilon_1} \tag{5}$$

where λ and ν are experimental constants. Through coordinate transformation, Equation 5 can be rewritten in the form below:

$$\frac{\varepsilon_1}{\sigma_1 - \sigma_3} = \lambda + \nu\varepsilon_1 \tag{6}$$

Equation 6 can be considered the primary function of $\varepsilon_1/(\sigma_1 - \sigma_3)$ and ε_1. Using this functional form, the orthogonal test data can be analyzed and sorted in a secondary analysis to derive the relevant parameters λ and ν. The sorting results are presented in Figure 13.

Figure 13 reveals that the parameters' linear fit correlation coefficients R^2 exceed 0.9, indicating a significant linear fit correlation. In Equation 6, the parameter ν represents

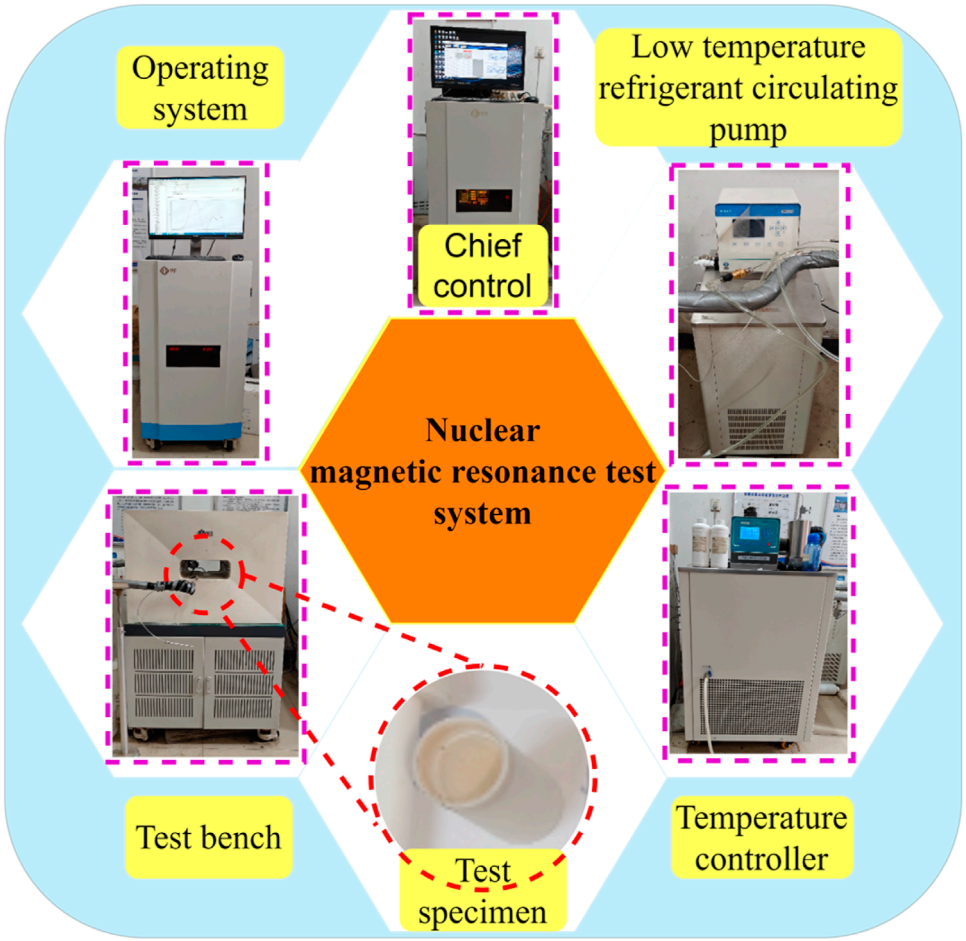

FIGURE 10
Configuration of nuclear magnetic resonance test system.

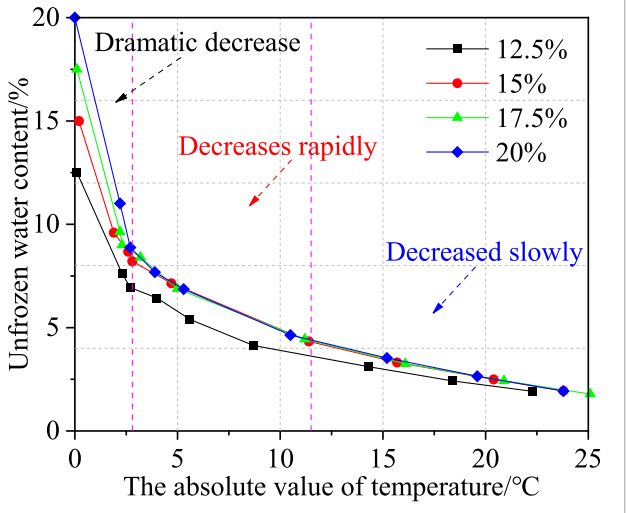

FIGURE 11
The evolution law of unfrozen water content of frozen calcareous clay with temperature under different water contents.

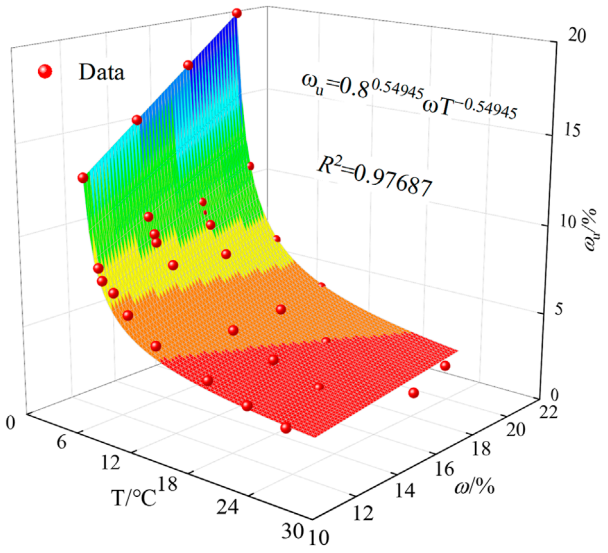

FIGURE 12
Formula fitting of unfrozen water content of frozen calcareous clay.

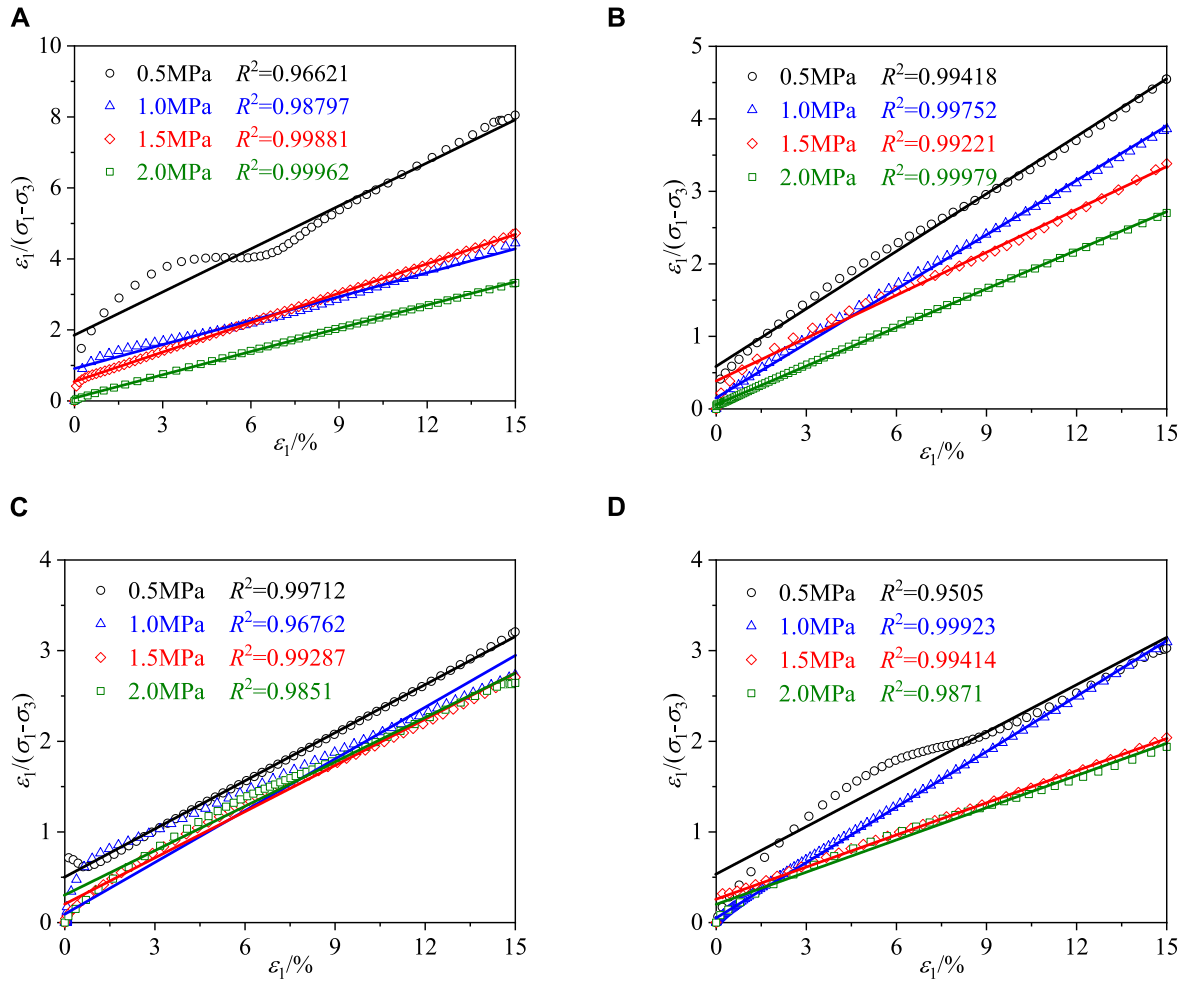

FIGURE 13
Parameter fitting of Duncan-Chang model at different temperatures. **(A)** T=−5°C. **(B)** T=−10°C. **(C)** T=−15°C. **(D)** T=−20°C.

TABLE 4 The fitting results of parameters v and λ.

Temperature / Confining pressure	−5°C		−10°C		−15°C		−20°C	
	v	λ	v	λ	v	λ	v	λ
0.5 MPa	0.40434	1.85361	0.2643	0.58672	0.17691	0.50178	0.17403	0.53485
1 MPa	0.22696	0.89906	0.24994	0.15103	0.19025	0.092	0.20388	0.0501
1.5 MPa	0.27674	0.543	0.19707	0.38472	0.17	0.20297	0.11809	0.25754
2 MPa	0.21791	0.08104	0.17736	0.05883	0.16315	0.30348	0.11841	0.20022

the slope of the straight line and λ is the intercept of the straight line on the vertical axis. The values of these parameters obtained from the fit are collated and presented in Table 4.

Table 4 indicates that the parameters v and λ vary with changes in confining pressure and temperature. The temperature affects the unfrozen water content within the sample, so it is assumed that the relationship between the parameters v and λ, the confining pressure, and the unfrozen water content can be expressed as Equations 7, 8:

$$v = f(\sigma_3, \omega_u) \tag{7}$$

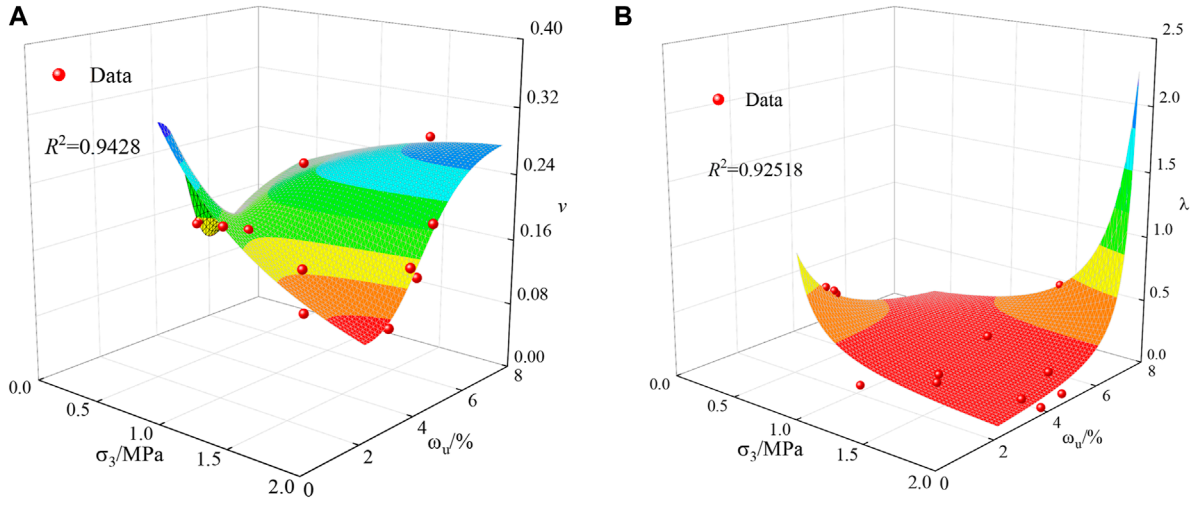

FIGURE 14
Parametric equation fitting of the Duncan-Chang model. **(A)** Fitting formula of parameter *v*. **(B)** Fitting formula of parameter *λ*.

$$\lambda = g(\sigma_3, \omega_u) \tag{8}$$

where $f(\sigma_3, \omega_u)$ and $g(\sigma_3, \omega_u)$ are functional relations related to confining pressure σ_3 and unfrozen water content ω_u.

The specific values of the unfrozen water content of the samples at four temperatures were calculated using Equation 4. These values were then fitted to the parameters v and λ by combining the data in Table 4. The results of this fitting process are illustrated in Figure 14.

It is observed that the binary nonlinear fitting correlation coefficients of parameters v and λ exceed 0.9, indicating a significant nonlinear fitting correlation. The fitted expressions are as follows:

$$v = \frac{0.5039 - 0.04621\sigma_3 - 0.33883\omega_u + 0.03993{\omega_u}^2 + 0.12461\sigma_3\omega_u}{1 + 0.38433\sigma_3 - 0.92555\omega_u + 0.18341{\sigma_3}^2 + 0.10091{\omega_u}^2 + 0.44398\sigma_3\omega_u} \tag{9}$$

$$\lambda = \frac{5.54723}{9.73223 - 2.7894\omega_u + 28.35811\sigma_3 - 2.05817\sigma_3\omega_u} \tag{10}$$

According to Equation 4, ω_u is a function of initial water content ω and temperature T. Accordingly, the relationship between parameters v, λ and confining pressure, temperature, initial water content can be expressed as Equations 11, 12:

$$v = F(\sigma_3, T, \omega) \tag{11}$$

$$\lambda = G(\sigma_3, T, \omega) \tag{12}$$

where $F(\sigma_3, T, \omega)$ and $G(\sigma_3, T, \omega)$ are functional relations that are related to the confining pressure σ_3, temperature T, and initial water content ω.

Introducing Equation 4 into Equation 9 and Equation 10, yields the following expression:

$$v = \frac{0.5039 - 0.04621\sigma_3 - 0.29973\omega T^{-0.54945} + 0.03125\omega^2 T^{-1.0989} + 0.11023\sigma_3\omega T^{-0.54945}}{1 + 0.38433\sigma_3 - 0.81874\omega T^{-0.54945} + 0.18341{\sigma_3}^2 + 0.07896\omega^2 T^{-1.0989} + 0.39274\sigma_3\omega T^{-0.54945}} \tag{13}$$

$$\lambda = \frac{5.54723}{9.73223 - 2.4675\omega T^{-0.54945} + 28.35811\sigma_3 - 1.82066\sigma_3\omega T^{-0.54945}} \tag{14}$$

5 Discussion

The relationship between the parameters (v, λ) of the Duncan - Chang model and the confining pressure, temperature, and initial water content has been deduced above. The prediction model for the strength of frozen calcareous clay under the influence of multiple factors can be established by combining Equations 13, 14 with Equation 5. To verify the precision of the model, the predicted curve is compared with the experimental results, as depicted in Figure 15. It can be noted that the experimental results are largely in accordance with the theoretical predictions. Only when the temperature is - 15°C and the confining pressure is 2 MPa does the correlation coefficient show a slight decline below 0.9. This deviation occurs because the deviatoric stress exhibits a quadratic increase when the axial strain reaches around 7%, causing the stress-strain curve to diverge from the expected hyperbolic shape. In light of the above - mentioned content, the veracity of the constitutive model of frozen calcareous clay based on the Duncan - Chang model, with the consideration of confining pressure, temperature and water content, is verified.

In previous research, the control variable method has usually been adopted for the analysis of this problem. The method of separately analyzing each factor by controlling variables one by one is inadequate for comprehensively understanding the strength characteristics of frozen calcareous clay under the interaction of multiple factors (Wang et al., 2017; Li et al., 2019; Fan et al., 2021).

Accordingly, this paper utilizes the design method of the orthogonal test to establish 16 groups of test conditions that represent multi - factor interaction levels, aiming to conduct a comprehensive exploration of the strength characteristics of frozen calcareous clay under different interaction levels. The utilization of

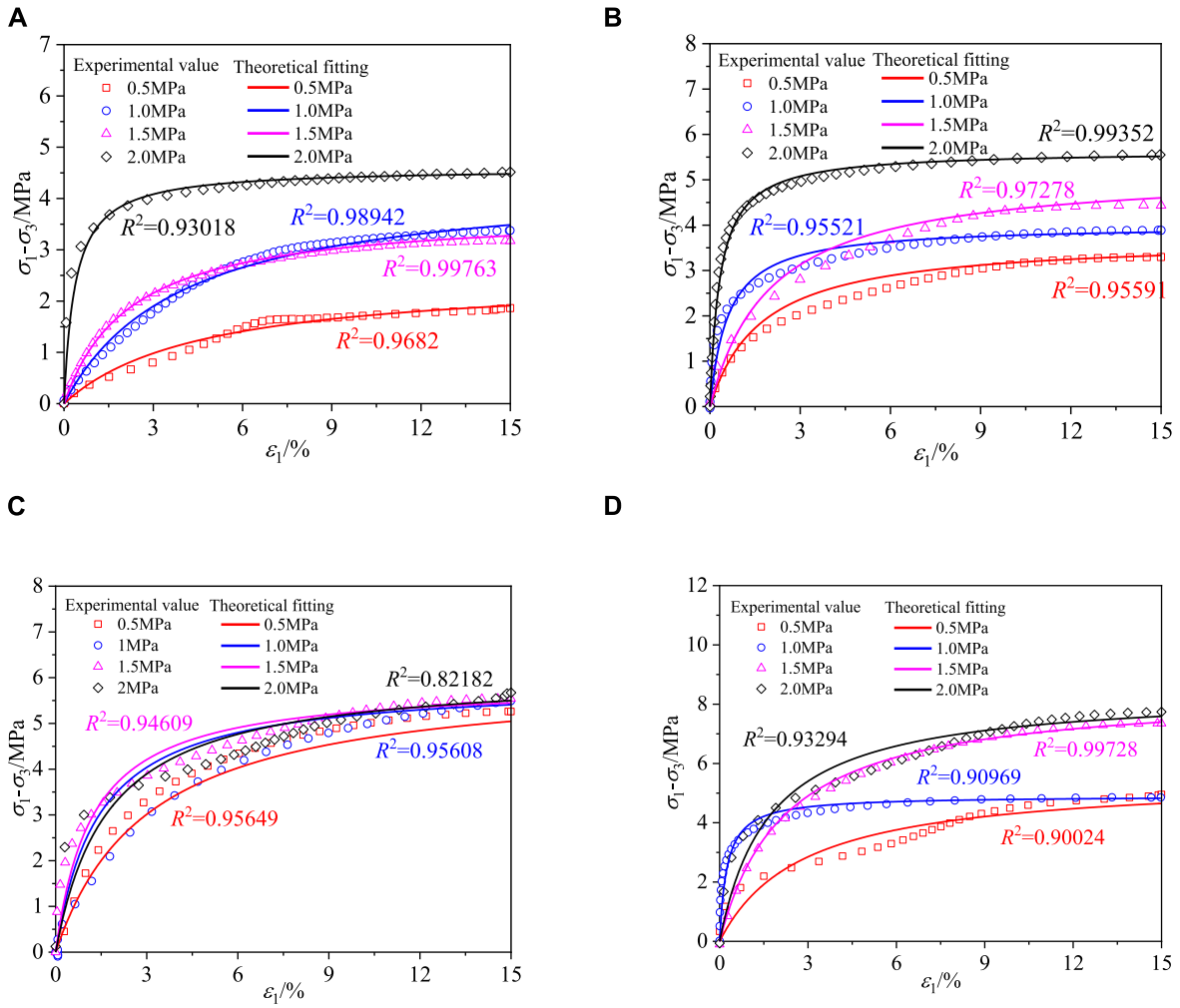

FIGURE 15
Comparison between theoretical curve and experimental data. **(A)** T=−5°C. **(B)** T=−10°C. **(C)** T=−15°C. **(D)** T=−20°C.

this research method has significantly enhanced our understanding of the strength characteristics of frozen calcareous clay, thereby laying a solid foundation for the construction of strength prediction models. The strength prediction model established in this study is of great significance in terms of the scientific rigour and accuracy of engineering design in cold regions.

However, due to time limitations, the range of factors investigated in this study is relatively narrow. We intend to expand the scope of the research in the future to include a larger number of factors that may affect the strength of frozen soil. The objective of this expanded research is to identify the key factors with the most significant impact and to modify and optimize the existing prediction models accordingly, aiming at achieving higher accuracy in predicting the strength of frozen soil in the natural environment.

6 Conclusion

This study employed a four-factor, four-level orthogonal test design to conduct conventional triaxial tests on calcareous clays, considering variables such as temperature, confining pressure, water content, and dry density. The research focused on the non-linear relationship between deviatoric stress and axial strain under different interaction levels and assessed the sensitivity of each factor to failure stress. From the experimental data, a theoretical formula for unfrozen water content was derived, leading to the development of a constitutive model for frozen calcareous clay based on the Duncan-Chang model. The main achievements of this article can be summarized as follows:

(1) The deviatoric stress-axial strain curves at different interaction levels all display strain-hardening characteristics. As the temperature decreases, the curves gradually shift from a weakly hardening type to a generally hardening type. The curves can be divided into elastic and elastic-plastic phases. Moreover, the slope of the elastic phase and the stress value at the inflection point show an increasing tendency with decreasing temperature and increasing confining pressure.

(2) When the confining pressure is maintained constant, the failure stress is negatively correlated with temperature. When the temperature is maintained constant, the failure stress is positively correlated with confining pressure. Sensitivity

analysis shows that the influence of each factor on failure stress is as follows: temperature > confining pressure > dry density > water content. Additionally, the influence of temperature and confining pressure on failure stress is markedly greater than that of water content and dry density.

(3) The evolution law curve of unfrozen water content can be divided into three phases: a sharp reduction phase, a rapid reduction phase, and a slow reduction phase. An intrinsic model of frozen calcareous clay considering temperature, confining pressure, and water content was constructed based on the Duncan-Chang model, with the unfrozen water content calculation formula acting as a link. The established modified constitutive model was verified by experimental data, showing its effectiveness in reflecting the stress-strain relationship of frozen calcareous clay under the influence of multiple factors.

Data availability statement

The datasets presented in this study can be found in online repositories. The names of the repository/repositories and accession number(s) can be found in the article/supplementary material.

Author contributions

JF: Data curation, Formal Analysis, Investigation, Methodology, Software, Validation, Writing–original draft. CR: Funding acquisition, Supervision, Writing–review and editing. HS: Funding acquisition, Supervision, Writing–review and editing. BW: Supervision, Writing–review and editing. ZW: Data curation, Investigation, Writing–review and editing. LG: Supervision, Writing–review and editing. ZT: Data curation, Investigation, Writing–review and editing. WL: Conceptualization, Methodology, Supervision, Writing–review and editing. DW: Data curation, Investigation, Writing–review and editing. XW: Data curation, Investigation, Writing–review and editing.

Funding

The author(s) declare that financial support was received for the research, authorship, and/or publication of this article. This work is financially supported by the National Natural Science Foundation of China (52404108), the National Natural Science Foundation of China (No. 51878005), the Research Activity Funding Project for Postdoctoral Researchers in Anhui Province (2023B726), the State Key Laboratory of Mining Disaster Prevention and Control, Shandong University of Science and Technology (JMDPC202403). The authors gratefully acknowledge financial support of the abovementioned agencies.

Conflict of interest

The authors declare that the research was conducted in the absence of any commercial or financial relationships that could be construed as a potential conflict of interest.

Generative AI statement

The author(s) declare that no Generative AI was used in the creation of this manuscript.

Publisher's note

All claims expressed in this article are solely those of the authors and do not necessarily represent those of their affiliated organizations, or those of the publisher, the editors and the reviewers. Any product that may be evaluated in this article, or claim that may be made by its manufacturer, is not guaranteed or endorsed by the publisher.

References

Bai, R., Lai, Y., Zhang, M., and Yu, F. (2018). Theory and application of a novel soil freezing characteristic curve. *Appl. Ther. Eng.* 129, 1106–1114. doi:10.1016/j.applthermaleng.2017.10.121

Chen, Y., Zhou, Z., Wang, J., Zhao, Y., and Dou, Z. (2021). Quantification and division of unfrozen water content during the freezing process and the influence of soil properties by low-field nuclear magnetic resonance. *J. Hydro.* 602, 126719. doi:10.1016/j.jhydrol.2021.126719

China Planning Press (2019). *The national standards compilation group of people's Republic of China. GB/T 50123—2019 standard for soil test method*. Beijing: China Planning Press.

Coal Industry Press (2011). *State administration of work safety.MT/T 593.1-2011 physical and mechanical properties test of artificial frozen soil*. Beijing: Coal Industry Press.

Cudmani, R., Yan, W., and Schindler, U. (2022). A constitutive model for the simulation of temperature-stress-and rate-dependent behaviour of frozen granular soils. *Géotechnique* 73 (12), 1043–1055. doi:10.1680/jgeot.21.00012

Deng, L. C., Li, X. Z., Chen, Y. W., Zhuang, Q. W., Zhu, L. H., and Zhang, C. (2023). Investigations on cutting force and temperature field of pick cutter based on single factor and orthogonal test methods. *Rock Mech. Rock Eng.* 56 (1), 619–645. doi:10.1007/s00603-022-03099-w

Dong, L., Wu, N., Zhang, Y., Liao, H., Hu, G., and Li, Y. (2023). Improved Duncan-Chang model for reconstituted hydrate-bearing clayey silt from the South China Sea. *Adv. Geo-Ene. Res.* 8 (2), 136–140. doi:10.46690/ager.2023.05.07

Duriez, J., and Vincens, É. (2015). Constitutive modelling of cohesionless soils and interfaces with various internal states: an elasto-plastic approach. *Comp. Geotech.* 63, 33–45. doi:10.1016/j.compgeo.2014.08.001

Fan, C., Zhang, W., Lai, Y., and Wang, B. (2021). Mechanical behaviors of frozen clay under dynamic cyclic loadings with freeze-thaw cycles. *Cold Reg. Sci. Tech.* 181, 103184. doi:10.1016/j.coldregions.2020.103184

Hai, M., Wang, M., Meng, S., Liu, Y., Ji, Y., Zhu, W., et al. (2024). Research on hydro-thermal coupling model of canal foundation soil based on particle grading curve predicting soil-water characteristic curve. *Case Stud. Ther. Eng.* 56, 104270. doi:10.1016/j.csite.2024.104270

He, P., Cao, H., Dong, J., Hou, G., Mu, Y., and Zhang, J. (2024). Experimental study on the effect of freeze-thaw cycles on the shear characteristics of frozen soil-composite geotextile interface. *Case Stud. Ther. Eng.* 54, 104011. doi:10.1016/j.csite.2024.104011

Hoyos, L. R., Velosa, C. L., and Puppala, A. J. (2014). Residual shear strength of unsaturated soils via suction-controlled ring shear testing. *Eng. Geol.* 172, 1–11. doi:10.1016/j.enggeo.2014.01.001

Horpibulsuk, S., Shibuya, S., Fuenkajorn, K., and Katkan, W. (2007). Assessment of engineering properties of Bangkok clay[J]. *Can. Geotech. J.* 44 (2), 173–187. doi:10.1139/t06-101

Hu, X. D., and Wang, J. T. (2013). The triaxial shear test of artificially frozen soils in tunnel construction of Hong Kong. *Appl. Mech. Mater.* 353, 1653–1656. doi:10.4028/www.scientific.net/AMM.353-356.1653

Jiang, B., Xia, W., Wu, T., and Liang, J. (2021). The optimum proportion of hygroscopic properties of modified soil composites based on orthogonal test method. *J. Clea. Prod.* 278, 123828. doi:10.1016/j.jclepro.2020.123828

Kong, Y., Xu, M., and Song, E. (2017). An elastic-viscoplastic double-yield-surface model for coarse-grained soils considering particle breakage. *Comp. Geotech.* 85, 59–70. doi:10.1016/j.compgeo.2016.12.014

Li, Q., Zhang, D., Li, P., Cui, K., and Jing, X. (2023). The small-strain stiffness of frozen clay soils at different temperatures and initial water contents: experimental study and predicted model. *Cold Reg. Sci. Tech.* 215, 103986. doi:10.1016/j.coldregions.2023.103986

Li, S., Wang, C., Xu, X., Shi, L., and Yin, N. (2019). Experimental and statistical studies on the thermal properties of frozen clay in Qinghai-Tibet Plateau. *Appl. Clay Sci.* 177, 1–11. doi:10.1016/j.clay.2019.05.002

Liao, M., Lai, Y., and Wang, C. (2016). A strength criterion for frozen sodium sulfate saline soil. *Canad. Geotech. J.* 53 (7), 1176–1185. doi:10.1139/cgj-2015-0569

Liu, M. D., and Carter, J. P. (2003). Volumetric deformation of natural clays. *Inter. J. Geomech.* 3 (2), 236–252. doi:10.1061/(ASCE)1532-3641(2003)3:2(236)

Long, H., Zhai, J., Zhang, Z., Zhao, Y., Zhang, K., and Zhang, A. (2024). Study on the effect of step ratio to temperature field of cut-fill transition in deep seasonal frozen soil region. *Case Stud. Ther. Eng.* 54, 104051. doi:10.1016/j.csite.2024.104051

Lu, D., Liang, J., Du, X., Ma, C., and Gao, Z. (2019). Fractional elastoplastic constitutive model for soils based on a novel 3D fractional plastic flow rule. *Comp. Geotech.* 105, 277–290. doi:10.1016/j.compgeo.2018.10.004

Ma, Q., Huang, K., and Ma, D. (2021). Energy absorption characteristics and theoretical analysis of frozen clay with pre-existing cracks under uniaxial compressive impact load. *Cold Reg. Sci. Tech.* 182, 103206. doi:10.1016/j.coldregions.2020.103206

Ni, P., Mei, G., Zhao, Y., and Chen, H. (2018). Plane strain evaluation of stress paths for supported excavations under lateral loading and unloading. *Soils Found.* 58 (1), 146–159. doi:10.1016/j.sandf.2017.12.003

Pardo Lara, R., Berg, A. A., Warland, J., and Parkin, G. (2021). Implications of measurement metrics on soil freezing curves: a simulation of freeze–thaw hysteresis. *Hydro. Proc.* 35 (7), e14269. doi:10.1002/hyp.14269

Shi, S., Zhang, F., Feng, D., and Xu, X. (2020). Experimental investigation on shear characteristics of ice–frozen clay interface. *Cold Reg. Sci. Tech.* 176, 103090. doi:10.1016/j.coldregions.2020.103090

Shi, Y., Kong, X., Ma, W., Zhang, L., Yang, C., and Mu, Y. (2024). Experimental study on the water and heat dynamic characteristics of silty clay at different depths under temperature gradient. *Case Stud. Ther. Eng.* 57, 104366. doi:10.1016/j.csite.2024.104366

Suebsuk, J., Horpibulsuk, S., and Liu, M. D. (2010). Modified Structured Cam Clay: a generalised critical state model for destructured, naturally structured and artificially structured clays. *Comp. Geotech.* 37 (7-8), 956–968. doi:10.1016/j.compgeo.2010.08.002

Sun, Z., Zhang, S., Wang, Y., Bai, R., and Li, S. (2022). Mechanical behavior and microstructural evolution of frozen soils under the combination of confining pressure and water content. *Eng. Geol.* 308, 106819. doi:10.1016/j.enggeo.2022.106819

Tatsuoka, F., Di Benedetto, H., Enomoto, T., Kawabe, S., and Kongkitkul, W. (2008). Various viscosity types of geomaterials in shear and their mathematical expression. *Soils Found.* 48 (1), 41–60. doi:10.3208/sandf.48.41

Wang, J., Nishimura, S., and Tokoro, T. (2017). Laboratory study and interpretation of mechanical behavior of frozen clay through state concept. *Soils Found.* 57 (2), 194–210. doi:10.1016/j.sandf.2017.03.003

Wen, Z., Ma, W., Feng, W., Deng, Y., Wang, D., Fan, Z., et al. (2012). Experimental study on unfrozen water content and soil matric potential of Qinghai-Tibetan silty clay[J]. *Environ. Earth Sci.* 66, 1467–1476. doi:10.1007/s12665-011-1386-0

Wu, H., Li, Z., Song, W., and Bai, S. (2021). Effects of superabsorbent polymers on moisture migration and accumulation behaviors in soil. *J. Clean. Prod.* 279, 123841. doi:10.1016/j.jclepro.2020.123841

Wu, J., Jing, H., Gao, Y., Meng, Q., Yin, Q., and Du, Y. (2022). Effects of carbon nanotube dosage and aggregate size distribution on mechanical property and microstructure of cemented rockfill. *Cem. Concr. Compos.* 127, 104408. doi:10.1016/j.cemconcomp.2022.104408

Wu, J., Jing, H., Yin, Q., Yu, L., Meng, B., and Li, S. (2020). Strength prediction model considering material, ultrasonic and stress of cemented waste rock backfill for recycling gangue. *J. Clean. Prod.* 276, 123189. doi:10.1016/j.jclepro.2020.123189

Wu, J., Wong, H. S., Zhang, H., Yin, Q., Jing, H., and Ma, D. (2024). Improvement of cemented rockfill by premixing low-alkalinity activator and fly ash for recycling gangue and partially replacing cement. *Cem. Concr. Compos.* 145, 105345. doi:10.1016/j.cemconcomp.2023.105345

Wu, J., Yang, N., Li, P., and Yang, C. (2023). Influence of moisture content and dry density on the compressibility of disturbed loess: a case study in Yan'an City, China. *Sustainability* 15 (7), 6212. doi:10.3390/su15076212

Wu, X. Y., Liang, Q. G., Niu, F. J., and Li, C. Q. (2017). Experimental study on shear strain hardening-softening classification of loess. *Chine J. Undergr. Space Eng.* 13 (06), 1457–1466.

Xu, X., Wang, B., Fan, C., and Zhang, W. (2020). Strength and deformation characteristics of silty clay under frozen and unfrozen states. *Cold Reg. Sci. Tech.* 172, 102982. doi:10.1016/j.coldregions.2019.102982

Xu, X., Wang, Y., Yin, Z., and Zhang, H. (2017). Effect of temperature and strain rate on mechanical characteristics and constitutive model of frozen Helin loess. *Cold Reg. Sci. Tech.* 136, 44–51. doi:10.1016/j.coldregions.2017.01.010

Xu, X. Z., Wang, J. C., and Zhang, L. X. (2001). *Frozen soil physics*. Editor X. Z. Xu (Beijing: Science Press), 105–107.

Yang, Y., Lai, Y., and Chang, X. (2010). Laboratory and theoretical investigations on the deformation and strength behaviors of artificial frozen soil. *Cold Reg. Sci. Tech.* 64 (1), 39–45. doi:10.1016/j.coldregions.2010.07.003

Zhang, M., Zhang, X., Lai, Y., Lu, J., and Wang, C. (2020). Variations of the temperatures and volumetric unfrozen water contents of fine-grained soils during a freezing–thawing process. *Acta Geotech.* 15, 595–601. doi:10.1007/s11440-018-0720-z

Zhang, T., Gao, Y., Liu, S., Yu, J., and Zhang, C. (2024). Experimental and numerical studies of breakage and fractal characteristics of silica sands in high-pressure triaxial tests. *Adv. Powder Technol.* 35 (7), 104548. doi:10.1016/j.apt.2024.104548

Zhang, T., Zhang, C., Song, F., Zou, J., Gao, Y., and Yang, W. (2023). Breakage behavior of silica sands during high-pressure triaxial loading using X-ray microtomography. *Acta Geotech.* 18 (10), 5195–5211. doi:10.1007/s11440-023-01866-9

Zhang, Y., Liu, S., Lu, Y., and Li, Z. (2021). Experimental study of the mechanical behavior of frozen clay–gravel composite. *Cold Reg. Sci. Tech.* 189, 103340. doi:10.1016/j.coldregions.2021.103340